Effects of cascading optical processes. Part II: Impacts on experimental quantification of sample absorption and scattering properties

Pathum Wathudura, $^{\diamond}$ Max Wamsley, $^{\diamond}$ Ankai Wang, $^{\Delta}$ Kexun Chen, † Samadhi Nawalage, $^{\diamond}$ Hui Wang, † , Shengli Zou, $^{\Delta}$, * and Dongmao Zhang $^{\diamond}$, *

[⋄] Department of Chemistry, Mississippi State University, Mississippi State, MS 39759, United States

[∆] Department of Chemistry, University of Central Florida, Orlando, FL 32816, United States.

[†] Department of Chemistry and Biochemistry, University of South Carolina, Columbia, SC 29208, United States

Abstract

In part I of the three companion articles we reported the effects of light scattering on experimental quantification of scattering extinction, intensity, and depolarization in solutions that contain only scatterers with no significant absorption and photoluminescence activities. The present work (Part II) studies the effects of light scattering and absorption on a series of optical spectroscopic measurements done on samples that contain both absorbers and scatterers, but not emitters. The experimental UV-vis spectrum is the sum of the sample absorption and scattering extinction spectra. However, the upper limit of the experimental Beer's-law-abiding extinction can be limited prematurely by the interference of forward scattered light. Light absorption not only reduces the sample scattering intensity, but also the scattering depolarization. The impact of scattering on sample light absorption is complicated, depending on whether the absorption of scattered light is taken into consideration. Scattering reduces light absorption along the optical path length from the excitation source to the UV-Vis detector. However, the absorption of the scattered light can be adequate to compensate the reduced light absorption along such optical path, making the impacts of light scattering on the sample total light absorption negligibly small (<10%). The latter finding constitutes a critical validation of the integrating-sphere-assisted resonance synchronous spectroscopic method for experimental quantification of absorption and scattering contribution to the sample UV-vis extinction spectra. The techniques and general guidelines provided in this work should help improve the reliability of optical spectroscopic characterization of nanoscale or larger materials, many of which are simultaneous absorbers and scatterers. The insights from this work are foundational for Part III of this series of works, which is on the cascading optical processes on spectroscopic measurements of fluorescent samples.

Introduction

Light and matter interactions such as light absorption, scattering, and emission are among the most Optical spectroscopic techniques including UV-vis, fascinating phenomena in nature. fluorescence, and light scattering are among the most taught techniques in STEM education. Moreover, these techniques are widely used measurement techniques in essentially every area of scientific inquiries and technological developments. ¹⁻⁶ The broad availability of commercial optical spectroscopic instruments have made the acquisition of UV-Vis, fluorescence, and scattering intensity spectra trivial. However, the reliable interpretation of experimental data can be challenging, especially for samples where two or more cascading optical processes can be triggered by individual incident photons.⁷ 11 Examples of cascading optical events include the re-scattering or absorption of scattered light, emission triggered by light absorption, and so on. Samples that exhibit such cascading optical events are ubiquitous in biological, chemical, environmental, and materials research. Indeed, optical spectroscopic measurements performed with samples that contain pure scatterers, simultaneous absorbers and scatterers, simultaneous absorbers and emitters, and finally simultaneous absorbers, scatterers, and emitters can all be complicated by such cascading optical processes. 11-13

In Part I of the three companion articles, we investigated the effects of light scattering on experimental quantification of sample scattering extinction, intensity, and depolarization. The first key learning is the interference of the forward scattered light on the UV-vis spectral acquisition, ¹⁴ which can compromise the general applicability of Beer's law for experimental quantification of scatterers' concentration or molar scattering coefficient. The second key finding is that the cascading light scattering complicates the correlation between scattering intensity and the scatterers' concentration. The scattering intensity initially increases with increasing scatterer concentration. However, when the scatterer's concentration is higher than a certain threshold,

increasing its concentration further reduces the sample scattering intensity due to scattering inner filter effect (IFE). The third key learning is that scattering depolarization monotonically increases with scatterers' concentration. However, the maximum achievable scattering depolarization remains less than unity even when the sample optical density is very high (e.g., >15). In other words, no isotropic light scattering can be achieved regardless of the degree of multiple scattering that occurs within the sample. Mechanistically this phenomenon is caused by the polarization dependence of the scattering IFE.¹⁴

The present work (Part II) is an extension of Part I and focuses on the effects of the cascading optical processes on optical spectroscopic measurement of solutions that contain both absorbers and scatterers, but not emitters. Samples that contain light absorbers, scatterers, and emitters will be discussed in Part III of the companion works. There are four major goals in this study. The first is to establish a general guideline for predicting the linear dynamic range (LDR) for the UV-vis spectra obtained with samples containing absorbers and scatterers. Such information is important for ensuring the reliability of using UV-vis spectra for experimental quantification of materials' molar extinction coefficient and for chemical quantifications. It is also relevant, considering the fact, that interference from forward scattered light can cause the measured UV-vis extinction to deviate from Beer's law, even when the measured UV-vis intensity is within the instrument LDR.¹⁴

Second, we wish to determine the effects of light absorption on the sample scattering depolarization (or interchangeably scattering anisotropy). Intrinsic scattering depolarization is a fundamental material property, and it depends on the scatterers' size, shape, and electronic structures. However, experimental quantification of scatterers' intrinsic scattering depolarization is challenging. Sample scattering depolarization increases with increasing sample

scatterers' concentration due to increasing multiplicative scattering.^{14, 15} However, impact of light absorption on sample scattering depolarization is unclear. Resolving this issue is necessary for reliable interpretation of sample scattering depolarization spectra and for understanding the impact of light absorption and scattering on the fluorescence depolarization. The latter will be studied in Part III of these companion articles.

Third, we wish to quantify the effects of scattering on the light absorption by chromophores in turbid samples. Conventional UV-vis spectral measurements allow one to quantify the light attenuation along its optical path from the excitation source to the detector. However, it provides no insight into the interplay of light absorption and scattering in the sample, such as the absorption of the scattered photons or the total number of photons absorbed by the sample. Quantifying the actual light absorbed by samples is important for photoactivated nanomaterial applications, including photocatalysis^{23, 24}, displays^{25, 26}, photothermal therapy,^{27, 28} and photodynamic therapy.^{29, 30} It is the total number of the absorbed photons that is responsible for photocatalyzed reactions, the temperature increase in the photothermal effects, and the singlet oxygen generation in photodynamic therapy. Therefore, it is critical to quantify the total light absorbed to determine the quantum efficiency in these applications.

Fourth, we wish to further examine the validity of the recent ISARS method for quantifying materials absorption and scattering extinction contribution to their UV-vis extinction spectrum. The ISARS method first quantifies the total fraction of the incident photons absorbed by the sample placed inside integrating sphere and subsequently uses a developed mathematical model by parameterizing ISARS intensity spectra to convert the ISARS-based absorbance to the sample conventional double-beam UV-vis absorbance.¹⁰ The effectiveness of the ISARS methods have been validated with optically transparent chromophores and fluorophores, but not with samples

that contain both scatterers and absorbers. If sample scattering has a significant impact on total light absorption, the mathematical model developed for converting the ISARS-based absorbance to the double-beam absorbance can be problematic. Fruitfully, we find that while scattering invariably reduces the light absorption along the optical path length used in conventional UV-vis measurements, its impacts on the total light absorption by the sample is negligibly small under the data acquisition conditions used in this work (*vide infra*).

Experimental Section

Materials and equipment. Carboxylate plain polystyrene nanoparticles (PSNPs) and dyed polystyrene nanoparticles (dPSNP) were purchased from Polysciences. The PSNPs with diameters of 50 nm (Cat#15913-10), 100 nm (Cat #16688), 200 nm (Cat #08216-15), and 380 nm (Cat #21753-15) were abbreviated as PSNP₅₀, PSNP₁₀₀, PSNP₂₀₀, and PSNP₃₈₀, respectively, while dyeimpregnated dPSNP with diameters of 300 nm (Cat# 24063-15), 530 nm (Cat #19815-15) and 1100 nm (Cat #19119-15) were abbreviated as dPSNP₃₀₀, dPSNP₅₃₀ and PSNP₁₁₀₀, respectively. The TEM images of plain PSNP have been shown before, ¹⁴ while that of dPSNPs are shown in the supporting information (Figure S1). KMnO₄ was obtained from Sigma-Aldrich and used as received. Nanopure water (18.2 M Ω cm⁻¹, Thermo Scientific) was used for all sample preparations. A Shimadzu UV-2600i spectrophotometer with an ISR 2600 integrating-sphere accessory (Duisburg, Germany) was used for all UV-vis and integrating-sphere UV-vis (ISUV) spectra. Resonance synchronous (RS) and linearly polarized resonance synchronous (LPRS) spectra were obtained using a FluoroMax-4 spectrofluorometer (Horiba Jobin Yvon, Edison, NJ) equipped with excitation and emission linear polarizers. A K-Sphere Petite integrating-sphere (Horiba PTI) with an internal diameter of 80 mm was used for ISARS spectral acquisition. All spectrofluorometerbased spectra were acquired with an integration time of 0.3 s and a bandwidth of 2 nm for both excitation and emission monochromators. The spectral intensity is the ratio between the signal from the sample detector and reference detector (S1/R1). All spectroscopic measurements are performed with a solution volume of 3 mL contained in a 1-cm square fluorescence cuvette.

Gold and silver nanoparticles. Gold nanoparticles (AuNPs) of three different sizes (35±2.4 nm; 54±4.4 nm; 91±8.6 nm) were synthesized using an established stepwise method.³¹ Colloidal silver nanoparticle (AgNPs) of three different sizes (38±2.5 nm; 59±4.1 nm; 84±7.5 nm) were also synthesized based on a published protocol.³² The synthesis procedures, TEM images, and particle size analysis are shown in the Supporting Information (Figures S2 and S3). The theoretical total extinction, absorption extinction, and scattering extinction spectra of the AuNPs and AgNPs were determined using a free, online Mie theory calculator from nanoComposix.³³

Computational simulation. The details of the computational model used is based on electrodynamics theory and the Monte Carlo method, which is discussed in a previous work.¹⁴ The instrumental parameters (cuvette size, solution height and volume, detector collection angle) used in the simulations were close to the experimental parameters. Particle size and incident wavelength were taken from the experiment. We also include the absorption of the nanoparticle, which was treated as zero when modeling polystyrene nanoparticles as pure scatterers. The scattering spectra were collected along directions perpendicular to the incident light direction using a collection angle of 2 degrees.

Results and Discussion

Sample characterization. Two representative types of samples that contain both light absorbers and scatterers are employed in this study. The first is a mixture of light absorbers and scatterers prepared by mixing carboxylate polystyrene nanoparticles (PSNPs), which are approximately pure scatterers with no significant absorption, ^{34, 35} and KMnO₄, a small molecular chromophore that is approximately a pure light absorber. ³⁶ For convenience, we refer to the samples containing both KMnO₄ and PSNP as PSNP/KMnO₄ solutions. Since those samples are used for probing the interplay between the sample absorptions and scattering, it is important to exclude the possibility of significant physiochemical interactions between KMnO₄ and PSNP to ensure the reliability of the spectral interpretation. ³⁷⁻⁴⁰

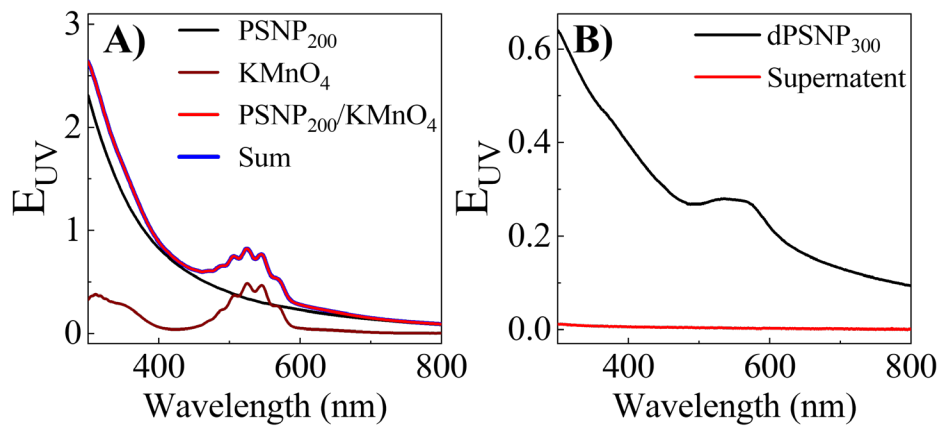


Figure 1: (A) Comparison of UV-vis spectra for (black) PSNP₂₀₀, (maroon) KMnO₄, (red) PSNP₂₀₀/KMnO₄, and (blue) the sum spectrum of PSNP₂₀₀ and KMnO₄. (B) Comparison of the UV-vis spectra of dPSNP₃₀₀ and its centrifugation supernatants.

There are strong optical interactions between the KMnO₄ and as-obtained PSNPs. The UV-vis spectrum of KMnO₄ mixed with as-obtained PSNPs deviates significantly from the mathematically additive spectrum of KMnO₄ and carboxylated PSNPs (**Figure S4**). Dialysis is effective to eliminate such spectral difference for samples prepared with PSNP₁₀₀, PSNP₂₀₀, and PSNP₃₈₀, as evident from the excellent agreement between the experimental UV-vis spectrum of PSNP/KMnO₄ solutions and the mathematic summation of UV-vis spectra of PSNP and KMnO₄

controls (**Figure 1A**), but not that with PSNP₅₀ (**Figure S4**). As a result, the KMnO₄ mixed with dialyzed PSNP₁₀₀, PSNP₂₀₀, and PSNP₃₈₀ are used as the PSNP/KMnO₄ solutions in subsequent studies.

The second type of samples used in this study are nanoparticles that are simultaneous light absorbers and scatterers with no significant emission activities. The model analytes include dPSNPs and plasmonic gold and silver nanoparticles (AuNPs and AgNPs, respectively). Unlike the plain PSNPs that are pure light scatterers in the probed wavelength region, dPSNPs contain light-absorbing dyes (*vide infra*) impregnated inside the polymer matrix. Experimental confirmation of the dye impregnation came from the total absence of the UV-vis feature in the spectrum obtained with the filtrate of the dPSNPs (**Figure 1B**). Fluorescence measurements confirm that dPSNPs have no significant fluorescence activities (**Figure S5**).

UV-vis extinction. Part I showed that forward scattered light interferes with the UV-vis spectral measurement, making the experimental scattering extinction spectrum deviate from Beer's law even when the sample theoretical extinction is within the instrument LDR. Theoretically, interference of forward scattered light is a general phenomenon in the UV-vis measurement for scatterer-containing samples. Eq. 1 correlates the sample experimental UV-vis extinction spectra $E_{UV}(\lambda)$ of solutions containing both absorbers and scatterers and its theoretical counterparts $E_T(\lambda)$, is defined by Eq. 2. Eq. 1 is derived based on a similar theoretical consideration for developing the mathematical equation for correlating the sample experimental and theoretical extinction for scattering-only samples.¹⁴ Substitution of Eq. 2 into Eq. 1 leads to Eq. 3, where the logarithm terms (the second term in Eq. 3) are identical to the equation for correlating experimental scattering extinction with the sample theoretical scattering extinction.

$$E_{UV}(\lambda) = -\log \frac{I_0(\lambda)10^{-E_T(\lambda)} + \eta(\lambda)I_{fS}(\lambda)10^{-A(\lambda)}}{I_0(\lambda)}$$
(1)

$$E_T(\lambda) = \varepsilon_S(\lambda)lC_S + \varepsilon_A(\lambda)lC_A = S(\lambda) + A(\lambda)$$
 (2)

$$E_{UV}(\lambda) = A(\lambda) - \log \frac{I_0(\lambda) 10^{-S(\lambda)} + \eta(\lambda) I_{fS}(\lambda)}{I_0(\lambda)}$$
(3)

 $I_0(\lambda)$, $I_{fS}(\lambda)$, and $\eta(\lambda)$ has been defined before. 14 $I_0(\lambda)$ is the intensity of the incident light. $I_{fS}(\lambda)$ is the forward scattered light without considering the absorption inner filter effect on scattered light, where $\eta(\lambda)$ is the fraction of forward scattered light reaching the detector. $\varepsilon_S(\lambda)$ and $\varepsilon_A(\lambda)$ is the sample scattering and scattering absorption, respectively. C_A and C_S are the concentration of the absorbers and scatterers, respectively. They are identical for analytes that are simultaneous light absorbers and scatterers. $A(\lambda)$ and $S(\lambda)$ are the sample absorbance and scattering extinctions.

$$E_{UV,UL}(\lambda) = \min\left(\frac{S_{UL}(\lambda)}{SER(\lambda)}, A_{UL}(\lambda)\right) \tag{4}$$

Eq. 3 shows that the experimental UV-vis spectrum can be approximated as sample theoretical extinction spectrum for calculating the analyte concentration or extinction coefficient only when forward scattered light is insignificant in comparison to $I_0(\lambda)10^{-S(\lambda)}$. In other words, the scattering extinction of turbid samples must be below $S_{UL}(\lambda)$, the upper limit of scattering extinction for scattering-only samples.¹⁴ Therefore, the upper limit of the Beer's-law-abiding experimental UV-vis extinction ($E_{UV,UL}(\lambda)$) of the samples that contain both light absorbers and scatterers can be predicted using Eq. 4, where the $A_{UL}(\lambda)$ is the upper LDR limit of the UV-vis instrument that is quantified using a pure light absorber. $SER(\lambda)$ is the sample scattering extinction vs. total extinction ratio at the excitation wavelength.

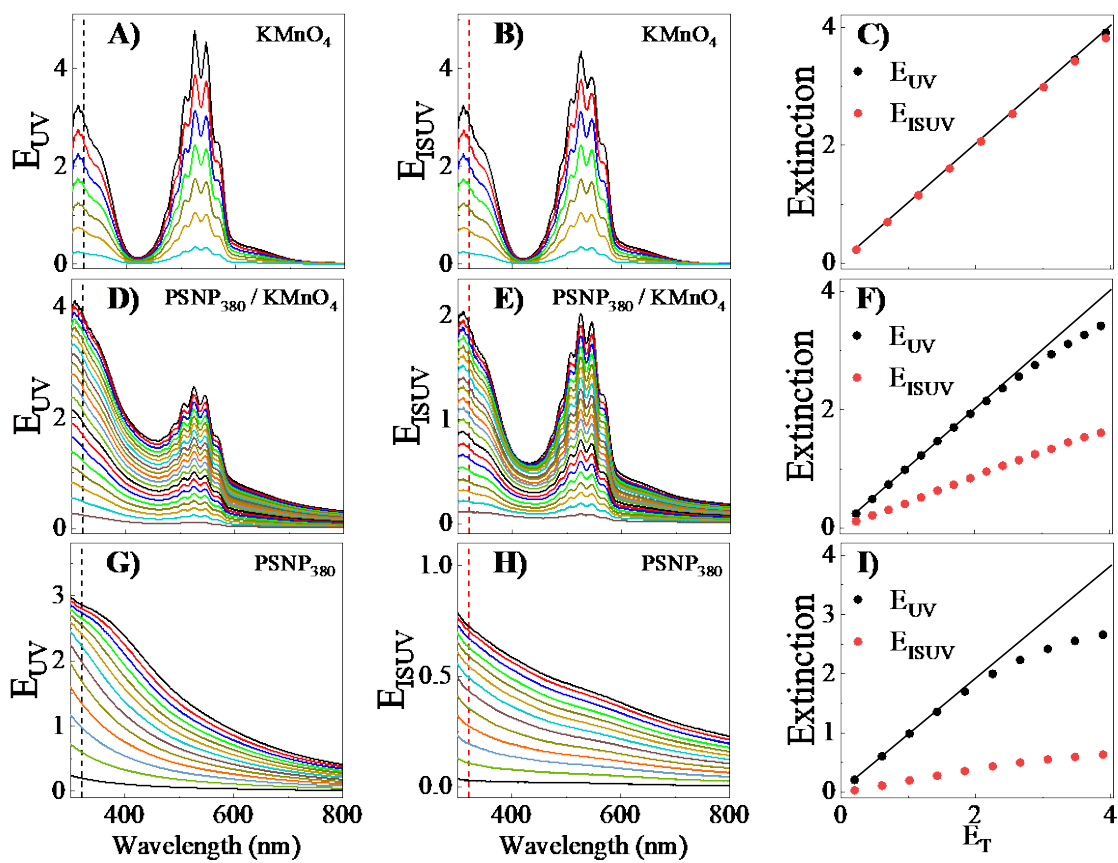


Figure 2: (A, D, G) UV extinction, (B, E, H) ISUV extinction, and (C, F, I) experimental UV and ISUV versus theoretical UV extinction at 320 nm for serial diluted (A, B, C) KMnO₄, (D, E, F) PSNP₃₈₀ / KMnO₄, and (G, H, I) PSNP₃₈₀. The extinction at 320 nm for the mixture shown is 75% PSNP (scattering) and 25% KMnO₄ (absorption). The data for a mixture with 85% PSNP and 15% KMnO₄ is shown in the Supporting Information (**Figure S6**).

Experimental validation of Eq. 4 for predicting the upper LDR limit of the sample UV-vis extinction are performed with three series of PSNP₃₈₀/KMnO₄ solutions with different scattering-to-extinction ratios (**Figure 2**). While the LDR range of the UV-vis spectra obtained with the conventional UV-vis and the ISUV for KMnO₄, an approximately pure molecular absorber, are the same, the upper LDR limit of UV-vis spectra obtained with the conventional UV-vis method is far higher than that using the ISUV method for the scattering samples. This result is not surprising because the IS collects all forward scattered light and is thereby much more sensitive than conventional UV-vis to the interference of light scattering in UV-vis spectral measurements. The excellent agreement between the conventional UV-vis and the ISUV spectra of KMnO₄

confirms that KMnO₄ is predominantly a light absorber with no significant scattering contribution to its UV-vis spectrum.

The instrument upper LDR limit of the spectrophotometer for a pure absorber is ~4 (Figure 2C), which is quantified using KMnO₄ at the excitation wavelength of 320 nm. The upper LDR limit at 320 nm for PSNP₃₈₀, a pure scatterer, is 1.8 (Figure 2I). The upper LDR limit of the experimental extinction of the PSNP₃₈₀/KMnO₄ mixtures with a SER at 320 nm of 0.75 and 0.85 are ~2.4 (**Figure 2**) and ~2.2 (**Figure S6**), respectively, which agree with that predicted using Eq. 4.

Apparently, the experimental UV-vis spectrum is equivalent to the sample theoretical extinction only when the measured extinction intensity is within the LDR defined with Eq. 4. In this case, one can use Beer's law to calculate the analyte extinction coefficient and/or concentration,

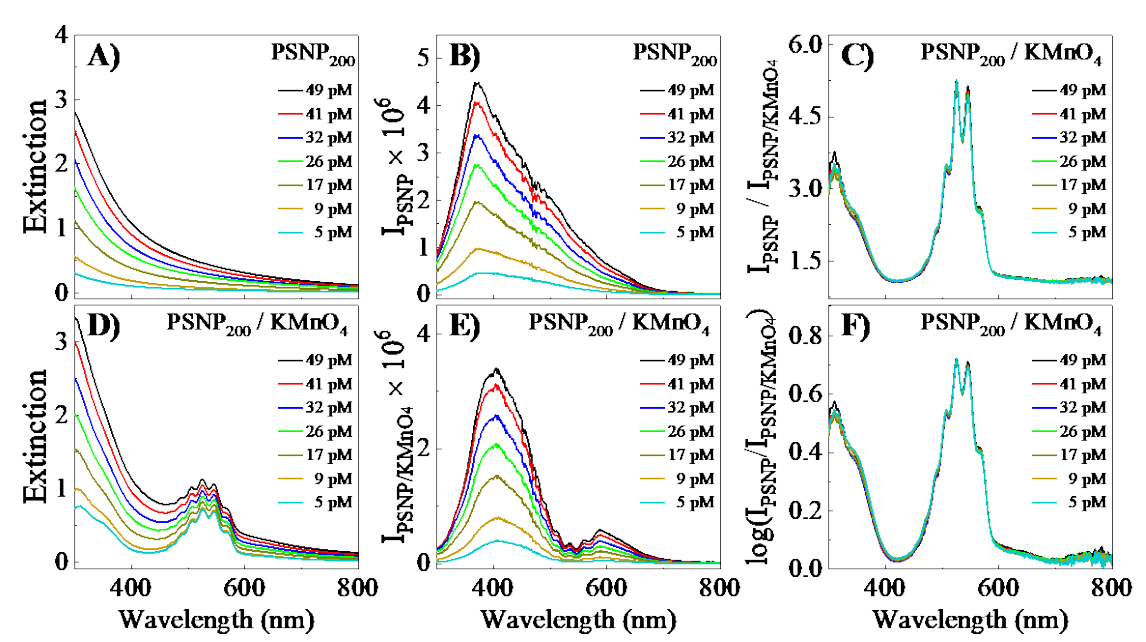


Figure 3: (A, D) UV-vis extinction spectrum and (B, E) scattering intensity of (A, B) PSNP₂₀₀ controls and (D, E) KMnO₄ /PSNP₂₀₀ solutions. (C) The ratiometric scattering intensity between PSNP control and the corresponding PSNP₂₀₀ / KMnO₄ solution where the KMnO₄ concentration is 272 μ M. (F) The logarithm of the ratiometric scattering spectra is also shown. Comparison of (F) the logarithm spectra and the UV-vis absorbance spectrum of the KMnO₄ control is shown in the Supporting Information (**Figure S7**).

and the sample UV-vis extinction spectrum is the sum of its absorption extinction and scattering extinction spectrum. The latter has significant implication for quantitative separation of scattering and absorption extinction contribution to the sample UV-vis extinction spectrum (*vide infra*).

Effect of light absorption on scattering intensity. The impact of light absorption on the scattering intensity was investigated by comparing the PSNP scattering intensities between a series of PSNP/KMnO₄ and their respective PSNP controls (**Figure 3**). All PSNP/KMnO₄ solutions have the same KMnO₄ concentration but differ in the PSNP concentration.

The scattering intensity of the KMnO₄-containing PSNP solutions are invariably lower than that of their respective PSNP controls in the wavelength region where KMnO₄ absorbs (**Figure 3(A-B) and 3(D-E)**). The higher the KMnO₄ absorbance is at the probed wavelength, the higher the scattering intensity ratio between the PSNP control and its corresponding PSNP/KMnO₄ solution (**Figure 3C**). Critically, these intensity ratios are totally independent of the PSNP concentrations and depend only on the KMnO₄ concentration (**Figure 3C**). The logarithm spectra (**Figure 3F**) of these intensity ratio spectra are remarkably similar to the UV-vis absorbance spectrum of KMnO₄ (**Figure S7**).

Mechanistically, KMnO₄-induced scattering intensity reduction occurs due to KMnO₄ absorption of the incident and scattered light, which is known as the absorption inner filter effect (IFE). Earlier works have demonstrated that absorption IFE on scattering intensity can be modelled with Eq. 5, where $I_{sca}^{abs}(\lambda)$ and $I_{sca}^{0}(\lambda)$ are the scattering intensity of the sample with and without light absorbers, respectively.³⁴ $A(\lambda)$ is the double-beam absorption extinction of the absorber-containing sample measured with a cuvette pathlength of $d_{ab}(\lambda)$, which is 1-cm in most UV-vis measurements, including the ones in this work. $d_{eff}(\lambda)$ is the effective absorption

pathlength of photons along the optical excitation and detection paths employed in the scattering intensity detection. For simplicity, we refer to $d_{eff}(\lambda)$ as the effective absorption pathlength.

$$I_{sca}^{abs}(\lambda) = I_{sca}^{0}(\lambda) 10^{-A(\lambda)d_{eff}(\lambda)/d_{ab}(\lambda)}$$
(5)

The effective absorption pathlengths $d_{eff}(\lambda)$ in the PSNP/KMnO₄ solutions are the same $(1.04\pm0.03~{\rm cm})$ and are close to 1-cm, as expected from the 1-cm square cuvette used in the scattering intensity measurement. Since the excitation and detection are centered at the middle of the cuvette, one would expect an effective pathlength of 1-cm $(0.5~{\rm cm})$ for excitation and $0.5~{\rm cm}$ for detection) for a perfectly aligned instrument under conditions that light scattering doesn't change the photon pathlengths. The fact that the effective pathlengths for the IFE correction are essentially independent of the sample scattering extinction indicates (Figure 3F) light scattering has no significant impact on the sample effective absorption pathlength or the total light absorption.

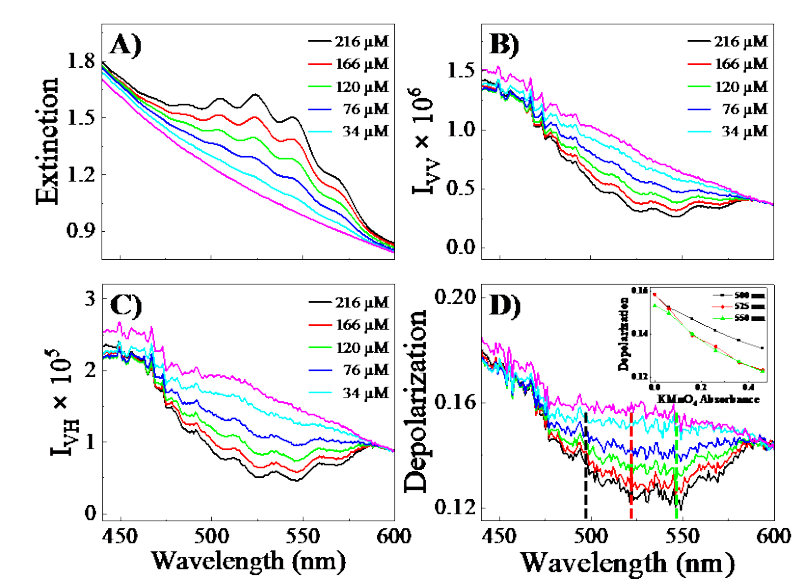


Figure 4: (A) UV-vis extinction, (B) LPRS VV, and (C) LPRS VH spectra of 11 pM PSNP₃₈₀ with varying concentration of KMnO₄ shown in the legend. (D) PSNP scattering depolarization in the PSNP₃₈₀/KMnO₄ solutions. The inset shows the scattering depolarization trend at the three labeled wavelengths.

Absorption on scattering depolarization. Light absorption reduces the sample scatterer depolarization, which is concluded on both experimental measurements (Figure 4) and computational modeling (Figure S8). The experimental samples used for studying the impact of light absorption on the sample scattering depolarization are a series of PSNP/ KMnO₄ solutions comprising of PSNPs at a constant concentration and KMnO₄ of varying concentrations (Figure 4). The sample scattering depolarization is calculated by dividing the sample LPRS VH spectra by the LPRS VV spectra and then multiplying the results by the instrument G-factor spectrum determined with a reported method.³⁴ This G-factor spectrum is to correct instrument bias in quantification of light with different polarizations. "VV" and "VH" refers to the combinations of the polarization directions of the excitation linear polarizer (the first letter) and the detector polarizer (the second letter). "V" represents that the light is polarized perpendicular to the instrument plane defined by the light source, sample chamber, and the detector, while "H" indicates that the light is polarized parallel to the instrument plane.

Both LPRS VV and VH intensities decrease with increasing KMnO₄ concentration in the wavelength region where KMnO₄ absorbs, which is consistent with the absorption inner filter effect discussed in the preceding section (Figure 3). The observation that scattering depolarization decreases with increasing KMnO₄ concentration indicates that light absorption attenuates the LPRS VH signal more effectively than LPRS VV intensity. Mechanistically, this phenomenon is due to the combination in the difference of the path lengths of the V and H polarized light, and the interconversion between the V and H polarized lights, as well as the polarization dependence of the scattering IFE.¹⁴ Since the intensity of V and H polarized light changes during each light scattering process, experimental determination of the average optical path length of the V and H

polarized light is currently impossible. Apparently, the polarized light that has a longer effective path length will have higher signal attenuation.

It has been well documented that light scattering enhances sample scattering and depolarization. 13, 21, 22 However, the impact of light absorption on scattering or fluorescence depolarization has, to our knowledge, not been reported. The finding that absorption reduces sample scattering depolarization further highlights the complexity of the cascading optical processes and their impacts on spectroscopic measurements for samples containing both scatterers and absorbers. This finding also raises questions about the potential interference of light absorption on fluorescence anisotropy measurements, a question that will be addressed in part III of this series of companion articles.

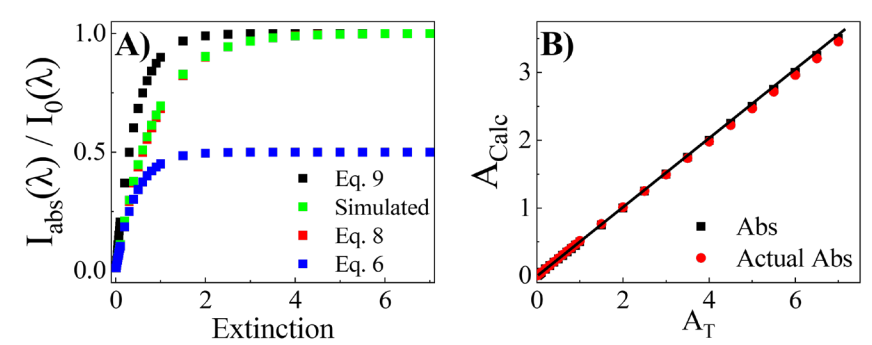


Figure 5: (A) Comparison of the modelled fraction of incident light absorbed with that calculated with Eq. 6, Eq. 8, and Eq. 9 as a function of the extinction intensity for samples with an AER = 0.5. (B) (black squares) The double-beam absorption extinction calculated using Eq. 8 and (red dots) the simulated actual light absorption extinction calculated using Eq. 10. The solid line is present to guide the view. Data for the AER from 0.1 to 0.9 with increments of 0.1 are shown in **Figures S8** and **S9**.

Effects of scattering on light absorption. Scattering has no effect on the measured sample absorption extinction if the sample experimental extinction is below the upper LDR limit defined with (Eq. 4). This conclusion is drawn based on the additivity of the sample scattering extinction spectrum and the absorption extinction spectrum (Figure 1A). However, experimental quantification of the impact of scattering on the intensity of the absorbed light in the conventional

UV-vis measurement is challenging. One may be tempted to use Eq. 6 and Eq.7, both derived from Eq. 2, for evaluating the absorbed $I_{abs}(\lambda)$ and scattered light $I_{sca}(\lambda)$, respectively. However, this approach invariably leads to overestimated scattering intensity and underestimated absorption intensities for samples that both absorb and scatter at the probed wavelength $(S(\lambda) > 0)$ and $A(\lambda) > 0$. This is because these equations fail to consider the absorption of the scattered light. The latter increases the absorbed photon intensity and reduces the scattering intensity predicted with Eq. 6 and Eq. 7, respectively.

$$I_{abs}(\lambda)/I_0(\lambda) = (1 - 10^{-(S(\lambda) + A(\lambda))}) \frac{A(\lambda)}{S(\lambda) + A(\lambda)}$$
(6)

$$I_{sca}(\lambda)/I_0(\lambda) = (1 - 10^{-(S(\lambda) + A(\lambda))}) \frac{S(\lambda)}{S(\lambda) + A(\lambda)}$$
(7)

There is no current experimental method for quantifying the intensity of absorbed or scattered light by a sample used in conventional UV-vis measurements, without perturbing light/matter interactions. However, the data shown in Figure 3 provides indirect evidence that addition of scatterers to absorbing samples have no significant impact on the total absorbed photons by the light absorbers. Otherwise, the sample absorption IFE imposed by KMnO₄ on the scattering intensity will also depend on the PSNP concentration, but not on the KMnO₄ concentration alone. This empirical observation is supported by the computational simulation performed for a series of analytes that are simultaneous light absorbers and scatters with absorption-to-extinction ratios (AER) varying from 0.1 to 0.9. The simulated sample extinction varies from 0.01 to 7, covering essentially all possible LDR range currently achievable with a modern UV-vis spectrophotometer. The simulated total light absorption was compared to that calculated using Eq. 6, Eq. 8, and Eq. 9 (Figure 5A, and Figure S9). Eq. 8 quantifies the fraction

of the excitation light absorbed by setting $S(\lambda) = 0$ in Eq. 6, while Eq. 9 quantifies the absorbed light in case one mistakes the experimental UV-vis spectrum as absorbance spectrum.

$$I_{abs}(\lambda)/I_0(\lambda) = 1 - 10^{-A(\lambda)} \tag{8}$$

$$I_{abs}(\lambda)/I_0(\lambda) = 1 - 10^{-E(\lambda)} \tag{9}$$

The modelled fraction of excitation light absorbed is significantly higher than that predicted with Eq. 6. This is expected because Eq. 6 considers only the light absorption along the optical path from the excitation source to the UV-vis detector, but not the absorption of the scattered light. On the other hand, the modelled light absorption is lower than that shown by Eq. 9, which is also expected because not all the scattered light can be absorbed. Fruitfully, the modelled total light absorption is close to that predicted with Eq. 8 across the entire simulated sample extinction range (**Figure 5A** and **Figure S9**), indicating that light scattering changes predominantly the locations where light absorption occurs in the solution, but not significantly the number of the absorbed photons. Both the computational simulation and the experimental data shown in Figure 3 indicate that for samples containing both simultaneous light absorbers and scatters, one can estimate the actual light absorption in the UV-vis measurement based on the sample absorption extinction alone without considering the possible scattering interference.

The simulation of the absorbed light also enables determination of the actual absorption sample extinction $A_{total}(\lambda)$ defined with Eq. 10 and shown in Figure 5B, where $I_{abs,total}(\lambda)$ is the intensity of total simulated light absorption, including the ones scattered before absorption. The differences between $A_{actual}(\lambda)$ and the UV-vis double-beam absorption extinction calculated with Eq. 8 are less than 10% for all the modelled samples (**Figure 5B, Figure S10**), which is negligible for most practical applications.

$$A_{actual}(\lambda) = -\log \frac{I_0(\lambda) - I_{a,total}(\lambda)}{I_0(\lambda)}$$
(10)

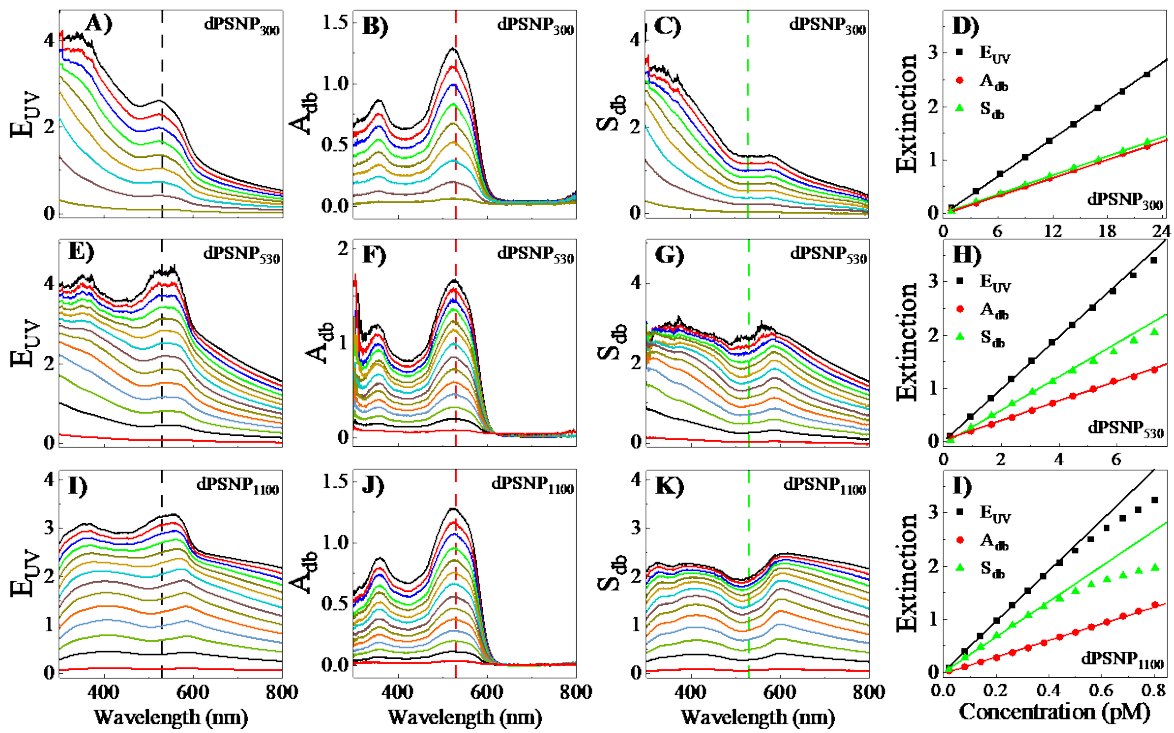


Figure 6: (A, E, I) Experimental UV-vis extinction, (B, F, J) double-beam absorption, and (C, G, K) scattering extinction spectra derived from ISARS measurements of (A, B, C) dPSNP₃₀₀, (E, F, G) dPSNP₅₃₀, and (I, J, K) dPSNP₁₁₀₀. (D, H, I) Extinction intensity at 520 nm as a function of dPSNP concentration. The linear lines are for guiding views.

Implication to ISARS quantification. ISARS is a recently developed method for quantification of materials double beam absorption and scattering extinction contribution to the sample UV-vis extinction spectrum.¹⁰ The key working principle underlying the ISARS method is that ISARS quantifies the total light absorption of the samples placed inside the integrating sphere. By including the effective stepwise absorption path length after each diffuse reflection by the integrating sphere, a mathematical model is developed for correcting the interference due to the multipath absorption caused by the IS diffuse reflection. ¹⁰ However, this stepwise absorption path length is quantified empirically through curve-fitting the experimental ISARS-based absorbance and double-beam absorbance for a series of optically transparent samples. While this

ISARS method has been validated with optically transparent samples, its utility to samples that contain both scatterers and absorbers has not been examined.

Herein, we provide an empirical validation to the ISARS method for experimental quantification of absorption and scattering extinction contribution to the UV-vis extinction spectra of three types of nanoparticles that are simultaneous absorbers and scatters, but with no significant fluorescence activities. The data obtained with dPSNPs are shown in Figure 6 and in Figure S11-S12, while the ones for AuNPs and AgNPs are in the supporting information (Figures S13 and S14). The double-beam UV-vis absorbance and scattering extinctions derived from the ISARS all exhibit excellent linearity with the nanoparticle concentration when the sample UV-vis extinction is within its LDR (Figure 6(D, H, I); Figure S13(F) and S14 (F)). Critically, the equation used for conversion of the sample ISARS-based absorbance to its double-beam absorbance is the one derived earlier with the optically transparent samples. 10 The linearity observed with these nanoparticle samples indicates that the effective stepwise light absorption path length inside the integrating sphere in the ISARS measurements is independent of sample scattering extinctions. Otherwise, the derived double-beam absorption extinction should depend on both the sample concentration and its scattering extinction, causing nonlinear dependence between absorption extinction and sample concentration.

The normalized absorption extinction spectra derived from the ISARS measurement for the dPSNPs of all three different sizes are in good agreement (**Figure S12**), which further validates the ISARS method. These dPSNPs contain the same dye molecules. Therefore, the shapes of the absorption extinction spectra of the dPSNP of different sizes should be approximately the same as observed. If scattering indeed changes the effective stepwise absorption path length in the ISARS method, the shapes of the ISARS-derived double-beam absorbance spectra of these dPSNPs must

differ significantly because the dPSNP of three different sizes differ significantly in their scattering features.

The ISARS-derived double-beam absorbance and scattering spectra for the plasmonic AuNPs and AgNPs are all in reasonable agreement with the theoretical spectra based on Mie theory calculations (**Figure S2** and **S3**).³³ The relatively small difference between the experimental and computed spectra is due likely to the fact that the theoretical spectra are calculated with the assumption that the nanoparticles are perfectly spherical with a uniform size; however, the synthesized AuNPs and AgNPs all have a relatively small, but finite size and shape distribution as shown with the TEM images.

It is critical to note that the linearity of the ISARS-derived double-beam absorbance doesn't guarantee the validity of the double-beam scattering extinction quantified using Eq. 2. To ensure the validity of the scattering extinction spectrum derived from the ISARS method, one must also ensure that the experimental UV-vis extinction must be equivalent to the sample theoretical extinction, i.e., the interference due to the forward scattered light is insignificant, as discussed earlier in this work. Otherwise, the ISARS measurement will provide an underestimated double-beam scattering extinction even when the deduced double-beam absorption extinction is accurate. Such an effect is evident from the dPSNP of three different sizes (Figure 6). The double-beam absorption extinction derived from the ISARS measurement maintains excellent linearity with the dPSNP concentration. In contrast, the sample UV-vis extinction spectra and the deduced double-beam scattering extinction begin deviating from their linear dependence on the dPSNP concentration when the sample experiment UV-vis extinction is higher than 2.5 and 2.2 for dPSNPs having a diameter of 510 nm and 1.1 μm, respectively (Figure 6D, 6H, 6I). These data indicates that for applications where only sample light absorption is of interest, a single sample

ISARS quantification of the sample double-beam absorbance can be adequate. However, for applications where sample scattering extinction is needed, one should ensure the experimental UV-vis extinction spectrum is within the sample LDR. The recommended approach for such applications is through serial dilution, as demonstrated herein with dPSNP (**Figure 6**) and the plasmonic AuNPs and AgNPs (**Figures S13-S14**).

Conclusion

The present work systematically investigated the impact of the cascading optical processes on experimental quantification of absorption and scattering properties of samples that contain absorbers and scatterers, but no emitters. A generalized mathematical equation was developed for predicting the upper LDR limit for the sample UV-vis spectral acquisition. experimental UV-vis extinction spectrum is equal to the sum of the absorption and scattering extinction spectrum when the forward scattering of the sample is small. While light absorption reduces not only the sample scattering intensity, and its scattering depolarization, the impact of scattering on the sample light absorption is much more complicated. Scattering invariably reduces the intensity of the light absorption along the linear optical path from the light source to the UVvis transmittance detector. However, the absorption of the scattered light can offset reduced light absorption along the linear optical path, making total light absorption by scatterer-containing samples comparable to that by the scatterer-free counterpart with the same absorption extinction. The latter provides critical validation to ISARS quantification of the double-beam light absorption and scattering extinction for samples with no significant forward-light-scattering interference in their UV-vis extinction measurements. These insights are important for improving the optical spectroscopic application of samples that contain both absorbers and scatterers. It is noted that

while the cascading optical process are inevitable in all light scattering samples, their impact on optical spectroscopic measurements depends not only on materials structure and composition, but also the instrument and measurement settings, including cuvette size. Nonetheless, whenever possible one should use diluted samples for experimental quantification of the optical properties of nanoscale or larger materials.

AUTHOR INFORMATION

Corresponding Authors

*E-mail: Dongmao Zhang <u>Dongmao@chemistry.msstate.edu</u>; Shengli Zou; <u>Shengli.zou@ucf.edu</u>

Notes

The authors declare no competing financial interest.

Supporting Information

TEM of dPSNP; synthesis and characterization of AuNP and AgNP; Effect of PSNP dialysis on PSNP and KMnO₄ interactions; UV-vis and scattering intensity spectra of dPSNP, PSNP, PSNP/KMnO₄ solutions; Example ISARS analysis of dPSNPs light absorption and scattering extinction; ISARS-derived double beam UV-vis absorbance and scattering spectra of dPSNP, AuNPs, and AgNPs; Simulated and absorbance spectrum of chromophore in scattering solutions.

Acknowledgement

This work was supported in part by the Center of Biomedical Research Excellence Program funded through the Center for Research Capacity Building in the National Institute for General Medical Sciences (P20GM103646), and by an NSF Grant (CHE 2203571). SZ is grateful for the support from NSF (DMR-2004546) and the Extreme Science and Engineering Discovery Environment (XSEDE) as the service provider through allocation to S. Zou. H.W. acknowledges the support by NSF under Grants CHE-2202928 and OIA-1655740. The content is solely the responsibility of the authors and does not necessarily represent the official views of the National Institutes of Health or National Science Foundation.

Reference

- 1. Agnarsson, B.; Lundgren, A.; Gunnarsson, A.; Rabe, M.; Kunze, A.; Mapar, M.; Simonsson, L.; Bally, M.; Zhdanov, V. P.; Höök, F., Evanescent Light-Scattering Microscopy for Label-Free Interfacial Imaging: From Single Sub-100 nm Vesicles to Live Cells. *ACS Nano* **2015**, *9* (12), 11849-11862.
- 2. Martindale, B. C. M.; Hutton, G. A. M.; Caputo, C. A.; Prantl, S.; Godin, R.; Durrant, J. R.; Reisner, E., Enhancing Light Absorption and Charge Transfer Efficiency in Carbon Dots through Graphitization and Core Nitrogen Doping. *Angewandte Chemie International Edition* **2017**, *56* (23), 6459-6463.
- 3. Huang, H.; Guo, Q.; Feng, S.; Zhang, C. e.; Bi, Z.; Xue, W.; Yang, J.; Song, J.; Li, C.; Xu, X.; Tang, Z.; Ma, W.; Bo, Z., Noncovalently fused-ring electron acceptors with near-infrared absorption for high-performance organic solar cells. *Nature Communications* **2019**, *10* (1), 3038.
- 4. Hou, S.; Exell, J.; Welsher, K., Real-time 3D single molecule tracking. *Nature Communications* **2020,** *11* (1), 3607.
- 5. Saini, A.; Messenger, H.; Kisley, L., Fluorophores "Turned-On" by Corrosion Reactions Can Be Detected at the Single-Molecule Level. *ACS Applied Materials & Interfaces* **2021**, *13* (1), 2000-2006.
- 6. Wamsley, M.; Peng, W.; Tan, W.; Wathudura, P.; Cui, X.; Zou, S.; Zhang, D., Total Luminescence Spectroscopy for Quantification of Temperature Effects on Photophysical Properties of Photoluminescent Materials. *ACS Measurement Science Au* **2022**.
- 7. Martens, H.; Nielsen, J. P.; Engelsen, S. B., Light Scattering and Light Absorbance Separated by Extended Multiplicative Signal Correction. Application to Near-Infrared Transmission Analysis of Powder Mixtures. *Analytical Chemistry* **2003**, *75* (3), 394-404.
- 8. Soos, M.; Lattuada, M.; Sefcik, J., Interpretation of Light Scattering and Turbidity Measurements in Aggregated Systems: Effect of Intra-Cluster Multiple-Light Scattering. *The Journal of Physical Chemistry B* **2009**, *113* (45), 14962-14970.
- 9. Oelkrug, D.; Brun, M.; Rebner, K.; Boldrini, B.; Kessler, R., Penetration of Light into Multiple Scattering Media: Model Calculations and Reflectance Experiments. Part I: The Axial Transfer. *Applied Spectroscopy* **2012**, *66* (8), 934-943.
- 10. Wamsley, M.; Wathudura, P.; Hu, J.; Zhang, D., Integrating-Sphere-Assisted Resonance Synchronous Spectroscopy for the Quantification of Material Double-Beam UV–Vis Absorption and Scattering Extinction. *Analytical Chemistry* **2022**, *94* (33), 11610-11618.
- 11. Nettles, C. B.; Zhou, Y.; Zou, S.; Zhang, D., UV–Vis Ratiometric Resonance Synchronous Spectroscopy for Determination of Nanoparticle and Molecular Optical Cross Sections. *Analytical Chemistry* **2016**, *88* (5), 2891-2898.
- 12. Vithanage, B. C. N.; Xu, J. X.; Zhang, D., Optical Properties and Kinetics: New Insights to the Porphyrin Assembly and Disassembly by Polarized Resonance Synchronous Spectroscopy. *The Journal of Physical Chemistry B* **2018**, *122* (35), 8429-8438.
- 13. Xu, J. X.; Hu, J.; Zhang, D., Quantification of Material Fluorescence and Light Scattering Cross Sections Using Ratiometric Bandwidth-Varied Polarized Resonance Synchronous Spectroscopy. *Analytical Chemistry* **2018**, *90* (12), 7406-7414.
- 14. Nawalage, S.; Wathudura, P.; Ankai, W.; Wamsley, M.; Zou, S.; Zhang, D., Effects of light scattering on optical spectroscopic measurements: Part I: impacts on the quantification of sample scattering extinction, intensity, and depolarizations. *Analytical Chemistry* **2022**, *Submitted*.
- 15. Xu, J. X.; Liu, M.; Athukorale, S.; Zou, S.; Zhang, D., Linear Extrapolation of the Analyte-Specific Light Scattering and Fluorescence Depolarization in Turbid Samples. *ACS Omega* **2019**, *4* (3), 4739-4747.

- 16. Germer, T. A., Polarized light scattering and its application to microroughness, particle, and defect detection. **1998**, *449* (1), 815-818.
- 17. di Stasio, S., Feasibility of an optical experimental method for the sizing of primary spherules in sub-micron agglomerates by polarized light scattering. *Applied Physics B* **2000**, 70 (4), 635-643.
- 18. Bescond, A.; Yon, J.; Girasole, T.; Jouen, C.; Rozé, C.; Coppalle, A., Numerical investigation of the possibility to determine the primary particle size of fractal aggregates by measuring light depolarization. *Journal of Quantitative Spectroscopy and Radiative Transfer* **2013**, *126*, 130-139.
- 19. Duncan, D. D.; Thomas, M. E., Particle shape as revealed by spectral depolarization. *Applied Optics* **2007**, *46* (24), 6185-6191.
- 20. Swami, M. K.; Patel, H. S.; Geethu, P.; Uppal, A.; Kushwaha, P. K.; Gupta, P. K., Effect of gold nanoparticles on depolarization characteristics of Intralipid tissue phantom. *Optics Letters* **2013**, *38* (15), 2855-2857.
- 21. Xu, J. X.; Siriwardana, K.; Zhou, Y.; Zou, S.; Zhang, D., Quantification of gold nanoparticle ultraviolet—visible extinction, absorption, and scattering cross-section spectra and scattering depolarization spectra: the effects of nanoparticle geometry, solvent composition, ligand functionalization, and nanoparticle aggregation. *Analytical Chemistry* **2018**, *90* (1), 785-793.
- 22. Mishchenko, M. I.; Travis, L. D. In *Polarization and Depolarization of Light*, Light Scattering from Microstructures, Berlin, Heidelberg, 2000//; Moreno, F.; González, F., Eds. Springer Berlin Heidelberg: Berlin, Heidelberg, 2000; pp 159-175.
- 23. Zhong, M.; Gagné, Y.; Hope, T. O.; Pannecoucke, X.; Frenette, M.; Jubault, P.; Poisson, T., Copper-Photocatalyzed Hydroboration of Alkynes and Alkenes. *Angewandte Chemie International Edition* **2021**, *60* (26), 14498-14503.
- 24. Ollis, D.; Silva, C. G.; Faria, J., Simultaneous photochemical and photocatalyzed liquid phase reactions: Dye decolorization kinetics. *Catalysis Today* **2015**, *240*, 80-85.
- 25. Zhmakin, A. I., Enhancement of light extraction from light emitting diodes. *Physics Reports* **2011**, *498* (4), 189-241.
- 26. Leung, V. Y. F.; Lagendijk, A.; Tukker, T. W.; Mosk, A. P.; Ijzerman, W. L.; Vos, W. L., Interplay between multiple scattering, emission, and absorption of light in the phosphor of a white light-emitting diode. *Optics Express* **2014**, *22* (7), 8190-8204.
- 27. Yang, W.; Guo, W.; Le, W.; Lv, G.; Zhang, F.; Shi, L.; Wang, X.; Wang, J.; Wang, S.; Chang, J.; Zhang, B., Albumin-Bioinspired Gd:CuS Nanotheranostic Agent for In Vivo Photoacoustic/Magnetic Resonance Imaging-Guided Tumor-Targeted Photothermal Therapy. *ACS Nano* **2016**, *10* (11), 10245-10257.
- 28. Li, D.; Zhang, G.; Xu, W.; Wang, J.; Wang, Y.; Qiu, L.; Ding, J.; Yang, X., Investigating the Effect of Chemical Structure of Semiconducting Polymer Nanoparticle on Photothermal Therapy and Photoacoustic Imaging. *Theranostics* **2017**, *7* (16), 4029-4040.
- 29. Sarıkaya, S. Y.; Yeşilot, S.; Kılıç, A.; Okutan, E., NIR BODIPY-Cyclotriphosphazene-Fullerene assemblies: Photophysiical properties and photosensitized generation of singlet oxygen. *Dyes and Pigments* **2019**, *162*, 734-740.
- 30. Lovell, J. F.; Chen, J.; Jarvi, M. T.; Cao, W.-G.; Allen, A. D.; Liu, Y.; Tidwell, T. T.; Wilson, B. C.; Zheng, G., FRET Quenching of Photosensitizer Singlet Oxygen Generation. *The Journal of Physical Chemistry B* **2009**, *113* (10), 3203-3211.
- 31. Zheng, Y.; Zhong, X.; Li, Z.; Xia, Y., Successive, Seed-Mediated Growth for the Synthesis of Single-Crystal Gold Nanospheres with Uniform Diameters Controlled in the Range of 5–150 nm. *Part. Part. Syst. Charact.* **2014**, *31* (2), 266-273.
- 32. Lin, X.; Lin, S.; Liu, Y.; Gao, M.; Zhao, H.; Liu, B.; Hasi, W.; Wang, L., Facile Synthesis of Monodisperse Silver Nanospheres in Aqueous Solution via Seed-Mediated Growth Coupled with Oxidative Etching. *Langmuir* **2018**, *34* (21), 6077-6084.
- 33. Oldenburg, S. J. Light scattering from gold nanoshells. Rice University, 2000.

- 34. Siriwardana, K.; Vithanage, B. C. N.; Zou, S.; Zhang, D., Quantification of the Depolarization and Anisotropy of Fluorophore Stokes-Shifted Fluorescence, On-Resonance Fluorescence, and Rayleigh Scattering. *Analytical Chemistry* **2017**, *89* (12), 6686-6694.
- 35. Xu, J. X.; Yuan, Y.; Zou, S.; Chen, O.; Zhang, D., A Divide-and-Conquer Strategy for Quantification of Light Absorption, Scattering, and Emission Properties of Fluorescent Nanomaterials in Solutions. *Analytical Chemistry* **2019**, *91* (13), 8540-8548.
- 36. Rideal, E. K.; Norrish, R. G. W., The photo-chemistry of potassium permanganate.-Part II. On the energetics of the photo-decomposition of potassium permanganate. *J Proceedings of The Royal Society A: Mathematical, Physical Engineering Sciences* **1923**, *103*, 366-382.
- 37. Pedersen, D. B.; Wang, S.; Paige, M. F.; Leontowich, A. F. G., Exploiting Near-Field Coupling between Closely Spaced, Gas-Phase, 10 ± 5 nm Ag Nanoparticles Deposited on NaCl To Observe the Quadrupolar Surface Plasmon Absorption. *The Journal of Physical Chemistry C* **2007**, *111* (15), 5592-5598.
- 38. Tung, B. S.; Khuyen, B. X.; Kim, Y. J.; Lam, V. D.; Kim, K. W.; Lee, Y., Polarization-independent, wide-incident-angle and dual-band perfect absorption, based on near-field coupling in a symmetric metamaterial. *Scientific Reports* **2017**, *7* (1), 11507.
- 39. Luu, D. H.; Tung, B. S.; Khuyen, B. X.; Tuyen, L. D.; Lam, V. D., Multi-band absorption induced by near-field coupling and defects in metamaterial. *Optik* **2018**, *156*, 811-816.
- 40. Wang, A.; Zou, S., Effects of Near- and Far-Field Coupling on the Enhancement Factor of the Radiative Decay Rate of Multiple Emitters Near a Silver Nanoparticle Sphere. *The Journal of Physical Chemistry C* **2022**, *126* (23), 9794-9802.

TOC graph

